PHYSICAL REVIEW ACCELERATORS AND BEAMS **23,** 072001 (2020)

Operation of normal-conducting rf cavities in multi-Tesla magnetic fields for muon ionization cooling: A feasibility demonstration

D. Bowring,[*] A. Bross, P. Lane, M. Leonova, A. Moretti, D. Neuffer, R. Pasquinelli,
D. Peterson, M. Popovic, D. Stratakis, and K. Yonehara
Fermi National Accelerator Laboratory, Batavia, Illinois 60510, USA

A. Kochemirovskiy
University of Chicago, Chicago, Illinois 60637, USA

Y. Torun
Illinois Institute of Technology, Chicago, Illinois 60616, USA

C. Adolphsen, L. Ge, A. Haase, Z. Li, and D. Martin
SLAC National Accelerator Laboratory, Menlo Park, California 94025, USA

M. Chung
Ulsan National Institute of Science and Technology, Ulsan 44919, Korea

D. Li and T. Luo
Lawrence Berkeley National Laboratory, Berkeley, California 94720, USA

B. Freemire and A. Liu
Euclid Techlabs, Bolingbrook, Illinois 60440, USA

M. Palmer
Brookhaven National Laboratory, Upton, New York 11973, USA

(Received 17 April 2020; accepted 11 May 2020; published 2 July 2020)

Ionization cooling is the preferred method for producing bright muon beams. This cooling technique requires the operation of normal conducting, radio-frequency (rf) accelerating cavities within the multi-tesla fields of dc solenoid magnets. Under these conditions, cavities exhibit increased susceptibility to rf breakdown, which can damage cooling channel components and imposes limits on channel length and transmission efficiency. We report, for the first time, stable high-vacuum, normal-conducting cavity operation at gradients of 50 MV/m in an external magnetic field of three tesla, through the use of beryllium cavity elements. This eliminates a significant technical risk that has previously been inherent in ionization cooling channel designs.

DOI: 10.1103/PhysRevAccelBeams.23.072001

I. INTRODUCTION

Scenarios for collisions of high-energy muons and the storage of muons as a neutrino beam source have been developed [1–4]. The physics reach of these machines relies on high-intensity muon beams, which in turn require the development of novel beam cooling techniques [5–7]. Building on this work, muon ionization cooling has recently been demonstrated for the first time [8].

A muon ionization cooling channel consists of strong-focusing magnets inducing high beam divergence within low-density, energy-absorbing media, and radio-frequency (rf) accelerating cavities to recover the longitudinal momentum lost by muons traversing the absorbing media. Because of the short muon lifetime, the cooling channel must be compact. In optimized channel designs, strong magnetic fields overlap high-gradient rf accelerating cavities. For example, the International Design Study for a future Neutrino Factory used 12–15 MV/m, 201 MHz rf cavities within two-tesla magnetic fields in its baseline design [2]. Some muon collider designs call for cooling

---

[*] dbowring@fnal.gov

channels with 805-MHz cavities operating at gradients above 23 MV/m in magnetic fields above ten tesla [9].

rf cavities operating within multi-tesla magnetic fields exhibit higher breakdown probability (BDP) per rf pulse at lower gradients, relative to operation in no magnetic field. The term "breakdown" here refers to an arc which abruptly shorts an rf cavity, draining its stored energy while generating heat, light, and x-rays. The damage incurred from breakdown in multi-tesla fields is also more severe than damage incurred during operation in no DC magnetic field [10,11]. The consequence of this increased breakdown probability is to limit the gradients at which cavities can reliably operate in magnetic fields. For example, in previous studies, the maximum achievable gradient for an 805-MHz copper cavity in the absence of a dc magnetic field was 40 MV/m; the same cavity was stable only below 14 MV/m when operated in a three-tesla field [12]. In the high-gradient limit, cavities can break down continuously and making stable operation impossible.

Simulations illustrate a consequence of this operational instability: artificially low cavity gradients depress the muon yield in an ionization cooling channel and, by extension, the maximum achievable luminosity [13,14]. Channel design options are constrained by this instability. For example, Rogers *et al.* limited cooling channel cavity gradients to 16 MV/m and designed magnet lattices to minimize the overlap of magnetic fields with rf cavities, with the explicit goal of reducing the risk of breakdown [13]. The work described here addresses this problem directly, by demonstrating a cavity design which is resistant to breakdown in conditions similar to those in an ionization cooling channel.

The specific physical cause of rf breakdown, and the dynamical processes relevant during breakdown, remain open questions. The breakdown probability of an accelerating structure seems to depend, though, on the following conditions: electron and ion interactions with the metal surface [10,15–17]; the intensity and distribution of cavity fields and surface currents [18,19]; and the extent of pulsed heating and resultant lattice strain [20,21]. These phenomena are interrelated and a given model of rf breakdown may incorporate several of them.

This work was performed at Fermilab's MuCool Test Area (MTA), a facility for R&D related to muon ionization cooling, including exploring methods of circumventing or suppressing rf breakdown in strong magnetic fields. Such methods include cleaning and polishing interior cavity surfaces to reduce the density of field emission sites, altering cavity geometry to minimize the effects of dark current and pulsed heating, and investigating the role of materials besides copper in the breakdown process [22–25].

A novel cavity design, and one uniquely suited for cooling muon beams, is to fill the cavity volume with high-pressure gas. This gas suppresses field emission during operation and minimizes breakdown effects [26]. Gradients above 60 MV/m have been demonstrated in a three-tesla external magnetic field using hydrogen gas at pressures above 1000 psia [27]. This relatively dense gas may also be used as a cooling medium. The work described here is complementary to that approach, and represents a feasible path to ionization cooling channels using a more conventional high-vacuum cavity design.

II. MODEL OF FIELD EMISSION AND PULSED HEATING

We employ the model of field emission and pulsed heating described in Ref. [28], which addresses the role of an external, DC magnetic field in the processes leading to breakdown. We apply this model to copper, beryllium and aluminum. Note that aluminum was not used in the experimental work described below; it is included here to illustrate a material with properties intermediate between those of copper and beryllium.

Cavities operating in cooling channel-like conditions in the MTA have exhibited dark current due to Fowler-Nordheim field emission [10,29]. The dark current density j_{FN} associated with this emission process is

$$j_{FN} = \frac{A_{\mathrm{FN}} \times (\beta E)^2}{\phi} \exp\left(-\frac{B_{\mathrm{FN}}\phi^{1.5}}{\beta E}\right), \tag{1}$$

with the coefficients $A_{\mathrm{FN}} = 1.54 \times 10^6$ A-eV/(MV)^2 and $B_{\mathrm{FN}} = 6.8 \times 10^3$ eV$^{-1.5}$ MV/m. Asperities, cracks, and other surface irregularities can enhance the electric field E by a factor $E \to \beta E$. Measurements in the MTA motivate $\beta = 385$ for this study, for copper surfaces with work function $\phi = 4.5$ eV [10]. For the pulsed heating analysis in this paper, we assume a work function of 5.0 eV for beryllium and 4.0 eV for aluminum.

In the absence of an external magnetic field, the trajectory of this dark current depends on the cavity rf phase. The impact sites of individual electrons are spread over a large area and the power density deposited by these electrons is relatively low. The role of the magnetic field is to focus this dark current into a "beamlet" that follows magnetic field lines (i.e., that has trajectory independent of the cavity's rf phase). Based on particle tracking simulations [30] with j_{FN} and β as inputs, our model employs the following relationship, illustrated in Fig. 1, between beamlet radius on impact (R, in μm) and solenoidal magnetic field strength B in tesla:

$$R = \frac{\xi I^{1/3}}{B}, \tag{2}$$

where I is the time-dependent beamlet current in μA and $\xi = 2.26 \times 10^5$ henry-μA$^{2/3}$/m is a model-dependent constant.

If a particular surface asperity is an efficient emitter of electrons, and if that emission persists over multiple rf

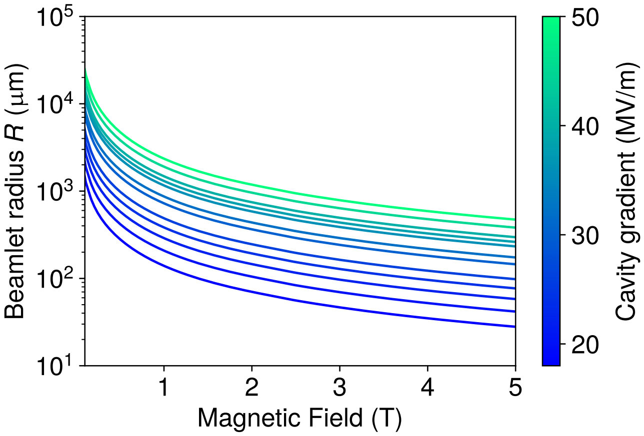

FIG. 1. Beamlet radius on impact vs magnetic field for a range of (copper) cavity gradients, assuming a prolate spheroidal emitter 1.77 μm wide and 62.0 μm long, consistent with $\beta = 385$. Space charge imposes a lower limit on beamlet size, even at very large magnetic fields.

periods, the beamlet impact site will undergo pulsed heating. The power density W ($\mathrm{W/m^3}$) delivered to the cavity wall is, using Eq. (2),

$$W = \frac{I(t)}{e\pi R^2}\frac{dE}{dz} = \frac{B^2 I^{1/3}}{\pi e \xi^2}\frac{dE}{dz} \tag{3}$$

for electron charge e and longitudinal stopping power dE/dz. W is the source term for the heat equation. Heat diffuses over a length scale $\delta = \sqrt{a\tau}$ during a time τ in a material with thermal diffusion constant a. In this case, $\tau = 20$ μs is the duration of the "flat-top" maximum average power during a single 32-μs rf pulse. Per Table II, the loaded Q-values associated with beryllium and copper endplates differ by almost 30%. The pulse length was not changed to accommodate these different Q-values. Instead, more power from the klystron was used to achieve equivalent gradients between measurements. The difference in pulse lengths associated with different coupling is accounted for in Equation (4) (see the Appendix for more information). The diffusion length δ is 48 μm for copper, 44 μm for aluminum, and 34 μm for beryllium. Beamlet-deposited heat diffuses away during the 0.1-second pause between pulses.

The heat equation can be solved in cylindrical coordinates using an RMS beamlet profile R per Eq. (2) and pulse duration τ, with Dirichlet boundary conditions on the radial coordinate and Neumann boundary conditions imposed on the longitudinal coordinate. The integral form of the heat equation gives the predicted local temperature rise ΔT due to beamlet heating:

$$\Delta T = \frac{a}{K}\int_0^\tau \int_0^d \int_0^R G_r G_z W(r,z,t) 2\pi r dr dz dt, \tag{4}$$

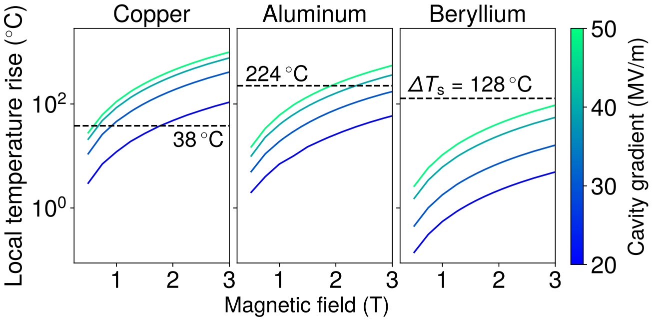

FIG. 2. Semi-log plot of local ΔT for Cu, Al, and Be cavities at various gradients and across a range of solenoidal magnetic field strengths. ΔT_s [Eq. (4)] is indicated in each plot by a horizontal, dashed line. Note that for Be, the local temperature rise is lower than ΔT_s for a broad range of gradients and magnetic fields.

where K is the thermal conductivity of the endplate, d is the RMS range of beamlet electrons into the endplate material, and G_r and G_z are one-dimensional Green's functions [31].

The temperature rise in Eq. (4) causes local stress in the vicinity of the beamlet impact site. This stress can exceed the yield stress σ_y of the cavity wall material. We define a "safe" temperature rise threshold ΔT_s, beyond which plastic deformation and surface damage may affect cavity behavior [32]:

$$\Delta T_s = \frac{(1-\nu)\sigma_y}{\epsilon\alpha} \tag{5}$$

for Poisson ratio ν, elastic modulus ϵ, and coefficient of linear thermal expansion α. For copper, $\Delta T_s = 38$ K and for beryllium, $\Delta T_s = 128$ K.

The dc magnetic field enhances the beamlet current density, increasing local heating and making any given beamlet more likely to cause local surface failure. Solving Eq. (4) numerically, the calculated local temperature rise is

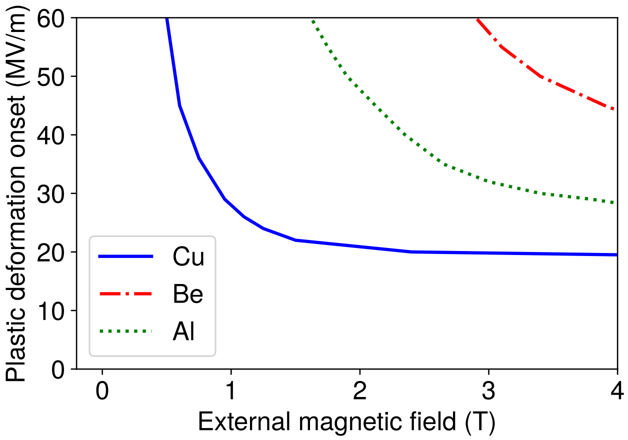

FIG. 3. Predicted cavity gradients vs external, solenoidal magnetic field strength, based on the beamlet pulsed heating model. Beryllium cavity walls should be less susceptible to fatigue from beamlet pulsed heating and should therefore operate at higher gradients relative to copper.

shown in Fig. 2 for several values of the cavity gradient as a function of external magnetic field strengths.

The intersection of the curves in Fig. 2 with the plastic deformation threshold ΔT_s gives the relationship between gradient and magnetic field shown in Fig. 3. The model suggests that materials like beryllium—with lower density and stopping power than copper—allow beamlets to exit the cavity with minimal energy deposition, reducing the power density available for pulsed heating. (As part of a full-scale muon accelerator, the possibility exists for dark current to be captured and transported through the beamline. MICE has demonstrated that appropriate placement of absorbers, which are required for ionization cooling, can limit the extent of this phenomenon and protect sensitive apparatus [33].) Moreover, beryllium has a higher plastic deformation threshold than copper and so should be more resistant to the effects of pulsed heating.

III. METHODS

Accordingly, an 805-MHz modular cavity was designed and built with removable walls, enabling a systematic comparison between copper and beryllium in the context of the pulsed heating model. The cavity is illustrated in Fig. 4; its design and operation are discussed in more depth in the Appendix.

The maximum stable operating gradient (SOG) is defined as the peak, on-axis electric field that results in an average breakdown rate of about one in 10^5 rf pulses, a limit based very roughly on the acceptable cavity uptime in the front-end of a muon accelerator. BDP is assumed to follow Poisson statistics. Counting breakdown events at a fixed gradient and 10-Hz rep rate, a measurement of SOG at 90% CL requires a minimum of 29 hours. A single high-power cavity run with full statistics, including time spent at lower gradients for cavity surface processing, can require several million pulses accumulated over two to four weeks of constant running. At the conclusion of each run, the cavity was disassembled and inspected inside a class-100 (ISO 5) clean room. Breakdown damage accumulated during the run was imaged using a digital microscope and a laser confocal scanning microscope, and the location of each damage site was recorded.

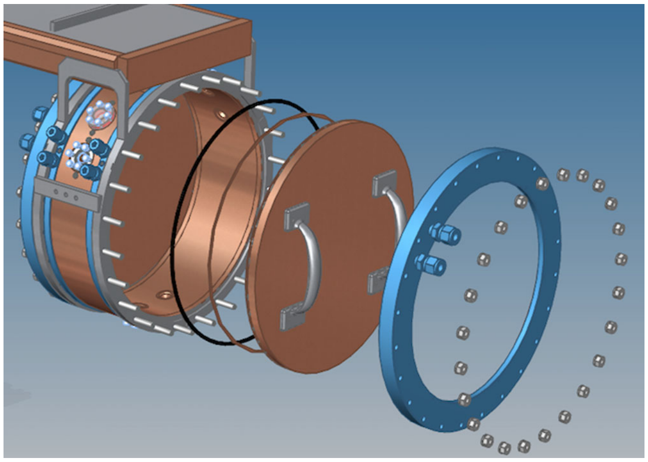

FIG. 4. Exploded view of cavity, illustrating assembly. From left to right, components include: cavity body; Viton O-ring for vacuum seal; annealed copper gasket for rf seal; modular endplate (made of copper or beryllium in this work); removable handles for endplate installation; stainless steel clamping ring with integrated water cooling lines; nuts to apply clamping pressure, threaded onto studs mounted on cavity body.

IV. RESULTS

Table I summarizes the stable operating gradients achieved with various configurations of the modular cavity. In particular, note that stable operation at 50 MV/m was possible in a three-tesla external magnetic field when using beryllium endplates. These results are compatible with the cooling channel designs for muon colliders given by, e.g., [9].

After establishing the SOG for beryllium in three tesla, a wide range of the parameter space was sampled with beryllium endplates at lower statistics. These results are summarized in the Appendix. In 3.5×10^6 total accumulated pulses, with magnetic fields between 0.5 and 3.5 T and gradients up to 48 MV/m, a total of three breakdown events were observed. It is likely that the beryllium surfaces continued to condition after the data in Table I were collected, making those surfaces even more resistant to breakdown.

Breakdown is possible within the cavity body, but also in the waveguide that delivers power to the cavity. The location of breakdown events was tracked using a series of pickup probes and directional couplers distributed throughout the MTA's rf apparatus. At gradients below 50 MV/m, breakdown was not observed in the waveguide. We note also that no breakdown damage was evident during a visual inspection of the waveguide elements after cavity operations concluded. At gradients above 50 MV/m, breakdown was observed in waveguide segments several meters upstream of the cavity body. By loading a section of the

TABLE I. Demonstrated SOG for various cavity configurations and external magnetic field strengths. At each operating point, the breakdown probability (BDP, sparks per pulse) is also shown. "Be/Cu" indicates operation with one beryllium and one copper endplate.

Material	B-field (T)	SOG (MV/m)	BDP ($\times 10^{-5}$)
Cu	0	24.4 ± 0.7	1.8 ± 0.4
Cu	3	12.9 ± 0.4	0.8 ± 0.2
Be	0	41.1 ± 2.1	1.1 ± 0.3
Be	3	$> 49.8 \pm 2.5$	0.2 ± 0.07
Be/Cu	0	43.9 ± 0.5	1.18 ± 1.18
Be/Cu	3	10.1 ± 0.1	0.48 ± 0.14

MTA's supply waveguide with sulfur hexafluoride, gradients above 50 MV/m were achieved. During three-tesla operation, a breakdown probability of 2.4×10^{-4} was observed at 56 MV/m in 25,000 pulses, using the beryllium endplates.

The cavity was run with one beryllium and one copper endplate. In this configuration, a three-tesla magnetic field limited the gradient to 10 MV/m. This result further illustrates the limitations on high-magnetic-field cavity performance imposed by copper surfaces.

Inspecting and cataloging breakdown damage after every high-power run has enabled the following observations. First, no breakdown damage was observed in the vicinity of the input power coupler, or anywhere in the cavity interior except for the endplate surfaces. The material of the endplates is evidently the limiting factor in cavity performance, helping to ensure that the measured breakdown limits do not stem from, for example, field enhancement in the region of the input power coupler [34].

The Modular Cavity design enables an observation for the first time that breakdown damage sites formed in the presence of a magnetic field are qualitatively different from those formed in a zero-tesla field. As shown in Fig. 5, damage on Cu surfaces during high-power operation is qualitatively different depending on whether the external magnetic field is absent or present. The solenoidal magnetic field induces a one-to-one correspondence of damage sites on opposite cavity walls, illustrated in Fig. 6. This is consistent with the beamlet focusing effects described above, in which charged particles follow magnetic field lines as they traverse the cavity.

Finally, we observed breakdown and damage to beryllium surfaces during $B = 0$ conditioning, but no additional damage was observed on beryllium surfaces after breakdown in three tesla. Figure 2 suggests that the gradients and magnetic fields required to cause plastic deformation of beryllium surfaces (and consequent surface damage) were not accessible during the course of this experimental program.

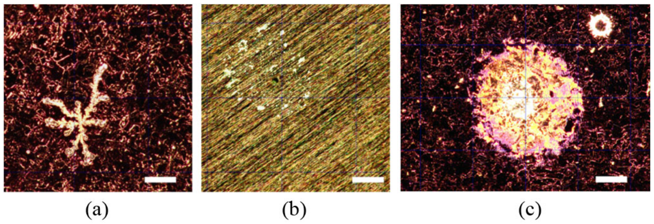
(a) (b) (c)

FIG. 5. Examples of breakdown damage on Be and Cu plates, observed after zero- and three-tesla runs, via digital microscopy. No new damage was evident on Be surfaces after three-tesla runs, so no images of this damage type are available. The white scale bar denotes 250 μm in all cases. (a) Damage on Cu from zero-tesla run; (b) Damage on Be from zero-tesla run; (c) Damage on Cu from three-tesla run.

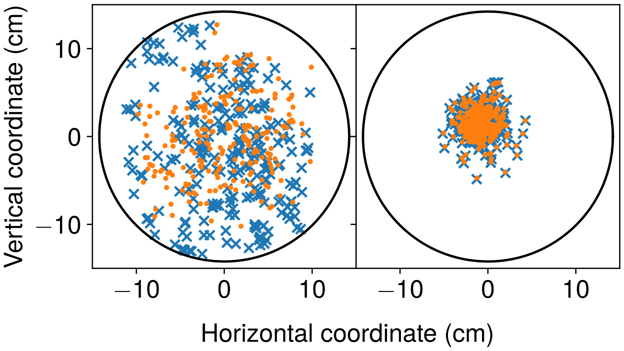

FIG. 6. Map of breakdown damage sites on copper cavity walls after high-power conditioning in zero-tesla external magnetic field (left) and three-tesla field (right). Damage locations are shown from the perspective of the "downstream" cavity wall in the foreground of Fig. 4; blue x's denote damage on the upstream wall and orange dots denote damage on the downstream wall. Breakdown damage in a three-tesla magnetic field exhibits a one-to-one correspondence between opposite cavity walls.

V. CONCLUSIONS

These results demonstrate the feasibility of muon ionization cooling channels that rely on evacuated rf cavities operating at gradients of tens of MV/m in multi-tesla external magnetic fields. Evacuated cavities and cavities loaded with high-pressure gas are evidently both viable options for cooling channel designs. In addition to relaxing gradient limits on cooling channel designs, the gradients achieved during this work illustrate the feasibility of high-power conditioning of cavity surfaces during beamline commissioning; this process relies on running cavities for prolonged periods at gradients significantly higher than the nominal design gradient.

The comparison between copper and beryllium was motivated by the pulsed heating model described above, and in particular the performance predictions illustrated by Fig. 2. The resistance of beryllium to breakdown is evident. However, we observed so few breakdown events during beryllium operation that it is difficult to directly verify the predictions of the pulsed heating model with high statistics. Future work could focus on aluminum. The pulsed heating model predicts that aluminum is more susceptible to breakdown than beryllium, so the measurement of SOG should happen at lower, more achievable gradients per Fig. 3. It is also a less brittle material than beryllium, and its machining and handling poses fewer health risks. Coating aluminum cavity surfaces with titanium nitride may minimize the secondary electron yield of those surfaces, reducing the risk of multipacting [24].

ACKNOWLEDGMENTS

The authors gratefully acknowledge Fernanda Garcia and the Fermilab Linac staff for their support of the MTA facility. The following people have provided valuable advice and support during the design and execution of this experimental program: Peter Garbincius, Jim Norem, and Alvin Tollestrup (Fermilab); Don Hartill (Cornell University); Dan Kaplan (Illinois Institute of Technology); Bob Palmer (Brookhaven National Lab); and Mike Zisman (Lawrence Berkeley National Lab). Fermilab is operated by Fermi Research Alliance, LLC under Contract No. DE-AC02-07CH11359 with the U.S. Department of Energy. This work was partially supported by grants from the U.S. Muon Accelerator Program (MAP) to the Illinois Institute of Technology. This research used resources of the National Energy Research Scientific Computing Center, a DOE Office of Science User Facility supported by the Office of Science of the U.S. Department of Energy under Contract No. DE-AC02-05CH11231.

APPENDIX: SUPPLEMENTAL MATERIAL

The cavity used in this study is an 805 MHz normal-conducting pillbox cavity, designed specifically to fit inside the 44-cm-diameter warm bore of the MTA superconducting solenoid magnet. The cavity was aligned with respect to the magnet bore such that the applied DC magnetic field was everywhere parallel to the electric field of the cavity's TM010 mode. The magnitude of the magnetic field $\vec{B}$ within the cavity volume was uniform to 6.7%, and its direction was parallel to the cavity's longitudinal z-axis with the mean of $(1 - B_z/|\vec{B}|) = 2.6 \times 10^{-4}$.

Cavity assembly and installation in the solenoid are illustrated in Figs. 4 and 7. The cavity body is built from copper. The circular, flat walls ("endplates") are clamped to the cavity body with a series of stainless steel fasteners. Annealed copper gaskets ensure good electrical contact between the cavity body and endplates, while a Viton o-ring provides a vacuum seal. This approach ensures consistent cavity parameters over multiple endplate mount/dismount cycles (Table II). rf power is coupled to the cavity via a custom-built narrow, rectangular waveguide which, outside of the constraints of the solenoid, transitions to standard WR-975. The waveguide design enables the cavity to be positioned to ensure the field uniformity condition described above. The input power coupler was designed using ACE3P [35], such that the peak surface electric field on the coupler is approximately five times smaller than the peak surface electric field on the cavity's longitudinal axis. This helps localize breakdown events to the cavity walls and keeps the input coupler from being a limiting factor of cavity performance [11].

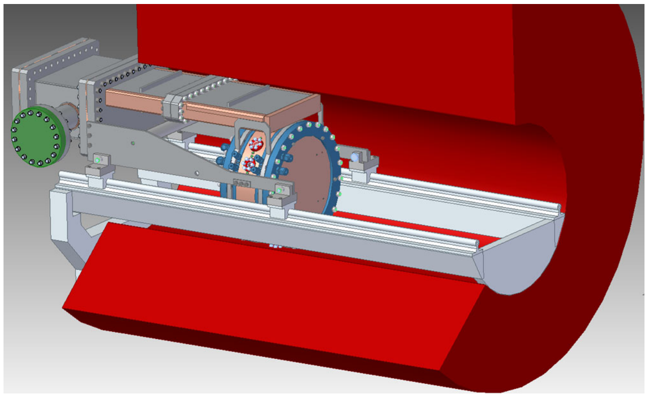

FIG. 7. Cavity mounted in MTA solenoid bore. False colors indicate: cut view of MTA solenoid (red); support rails (silver); vacuum pumping port (dark green); rf pickup and instrumentation ports (red).

TABLE II. Operating parameters for the Modular Cavity. Quoted uncertainty in reported values is the standard deviation across mount/demount endplate cycles, giving an indication of repeatability of experimental conditions. The cavity length is based on a $\pi/2$ phase advance for $v/c \approx 0.85$ muon beams.

	Cu walls	Be walls	Units
f_0	804.5 ± 0.1	804.48 ± 0.09	MHz
Q_0	23500 ± 900	16000 ± 2000	
Q_L	11100 ± 400	8700 ± 700	
Length	10.44	10.44	cm
Inner radius	14.2	14.2	cm
Base vacuum	10^{-8}	10^{-8}	Torr
Stored energy at 50 MV/m	20	20	J

Endplate surfaces were machined to better than 0.3 μm surface roughness and then coated with 20–60 nm of titanium nitride, with post-coating measured surface roughness $R_a = 0.29 \pm 0.02$ μm. Experience with the electropolishing of 201 MHz copper cavities suggests that smooth, polished surfaces help to suppress breakdown rates in ionization cooling channel contexts [22]. More work is needed in order to better understand the effect of surface quality on this specific cavity.

Interior cavity surfaces and endplate walls are coated with ≥ 20 nm of titanium nitride, with the goal of suppressing secondary electron yields. This reduces the risk of resonant electron loading (multipacting) and associated gradient limits [36,37].

The cavity is heavily instrumented. 3.38-cm ConFlat ports on the cavity body are mounting points for two inductive rf pickup probes used to measure cavity gradient. Two optically transparent windows are also mounted to the cavity body in this manner; attaching optical fibers to these windows allows for the detection of visible light during breakdown, via coupled photomultiplier tubes. Resistance temperature detectors (RTDs) are attached at multiple points around the cavity, in order to continually monitor the temperature of the cavity body and each endplate at multiple points. A control loop regulates the temperature of cooling water circulating in the cavity body and endplates, maintaining the temperature measured by the RTDs below

TABLE III. Sampling of the available operating parameters (solenoid field B and cavity gradient E) for the Modular Cavity with beryllium endplates. Three sparks were collected during this survey, indicating that the cavity continued to condition and higher gradients may be achievable. "0/100k" indicates zero sparks observed during 10^5 rf pulses.

	E (MV/m)					
B (T)	10	20	30	40	45	48
0.5	0/100k	0/100k	0/100k	0/200k	0/200k	2/300k
1.0	0/100k	0/100k	0/100k	0/200k	0/100k	0/300k
2.0	0/100k	0/100k	0/100k	0/100k	0/100k	1/300k
3.5	0/100k	0/100k	0/100k	0/100k	0/100k	0/300k

30°C and the temperature difference between endplate center and edges below 2.8°C. Vacuum pressure in the cavity is monitored by an ion gauge, coupled to the vacuum pumping port shown in Fig. 7. Gauges at and "upstream" of the vacuum manifold allow for the estimation of cavity pressure when the solenoid is energized and the main ion gauge is inoperable. Finally, radiation from the cavity is monitored by fast scintillators, a sodium-iodide counter, and various photomultiplier tubes and slower monitors positioned around the experimental hall. The "fast" counters are plastic scintillator (BC408), coupled to a Hamamatsu H10721-01 photomultiplier tube. These counters are used to monitor dark current. Signal timing is calibrated below 0.5 ns to enable observations of correlation between cavity-based radiation and the rf phase. Fast signals of this type—also including forward power and rf pickup voltage—are tracked and recorded by a bank of oscilloscopes with sampling rates up to 2×10^{10} samples per second.

The cavity was run with three endplate configurations and in magnetic field strengths between zero and three tesla, summarized in Tables I and III. During operation, LabVIEW-based run control software [38] increments forward power to the cavity at a predetermined ramp rate, typically $+0.2$ dB every fifteen seconds. Breakdown is detected by the logical OR of three signals: time derivative of an rf pickup probe signal above a predetermined threshold; time derivative of reflected power above a predetermined threshold; and the detection of light inside the cavity. When this logical condition is met, forward power is reduced by 3 dB and gradually reramped to the previous setpoint. Waveforms during breakdown (and, during normal operation, on the order of every 10^5 rf pulses) are recorded and stored to disk, along with logfiles detailing operating conditions before and during breakdown.

Above, we describe the performance of the cavity with copper and beryllium endplates operating at zero and at three tesla, for gradients up to 50 MV/m. After establishing the SOG for beryllium in three tesla, a wide range of the parameter space was sampled with beryllium endplates at lower statistics. These results are presented in Table III. Only three breakdown events were observed during the course of this survey, likely because the temperature rise limit for plastic deformation of beryllium was not accessible during this experimental program.

[1] S. Geer, Neutrino beams from muon storage rings: Characteristics and physics potential, Phys. Rev. D **57**, 6989 (1998).

[2] R. J. Abrams *et al.* (IDS-NF), International design study for the neutrino factory, arXiv:1112.2853.

[3] J. Delahaye, C. Ankenbrandt, A. Bogacz, S. Brice, A. Bross, D. Denisov, E. Eichten, P. Huber, D. Kaplan, H. Kirk *et al.*, Enabling intensity and energy frontier science with a muon accelerator facility in the U.S.: A white paper submitted to the 2013 U.S. community summer study of the division of particles and fields of the American Physical Society, arXiv:1308.0494.

[4] R. Palmer, Muon colliders, in *Reviews of Accelerator Science and Technology: Volume 7: Colliders* (World Scientific, Singapore, 2014), pp. 137–159.

[5] A. Skrinskii and V. Parkhomchuk, Methods of cooling beams of charged particles, Sov. J. Particles Nucl. (Engl. Transl.) **12** (1981).

[6] D. Neuffer, Principles and applications of muon cooling, Part. Accel. **14** (1983).

[7] D. Neuffer, Comments on ionization cooling channels, J. Inst. **12**, T09004 (2017).

[8] M. Bogomilov, R. Tsenov, G. Vankova-Kirilova, Y. P. Song, J. Y. Tang, Z. H. Li, R. Bertoni, M. Bonesini, F. Chignoli, R. Mazza, V. Palladino *et al.*, Demonstration of cooling by the Muon Ionization Cooling Experiment, Nature (London) **578**, 53 (2020).

[9] D. Stratakis, R. C. Fernow, J. S. Berg, and R. B. Palmer, Tapered channel for six-dimensional muon cooling towards micron-scale emittances, Phys. Rev. Accel. Beams **16**, 091001 (2013).

[10] J. Norem, V. Wu, A. Moretti, M. Popovic, Z. Qian, L. Ducas, Y. Torun, and N. Solomey, Dark current, breakdown, and magnetic field effects in a multicell, 805 MHz cavity, Phys. Rev. Accel. Beams **6**, 072001 (2003).

[11] D. Bowring, D. Peterson, A. Moretti, A. Kochemirovskiy, D. Stratakis, M. Palmer, B. Freemire, M. Leonova, A. Haase, P. Lane *et al.*, RF breakdown of 805 MHz cavities in strong magnetic fields, in *Proceedings, 6th International Particle Accelerator Conference (IPAC 2015): May 3-8, 2015* (JACoW Publishing, Richmond, VA, USA, 2015), p. MOAD2, http://accelconf.web.cern.ch/IPAC2015/doi/JACoW-IPAC2015-MOAD2.html.

[12] J. Norem, A. Bross, A. Moretti, Z. Qian, D. Huang, Y. Torun, R. Rimmer, D. Li, and M. Zisman, Recent RF results from the MuCool test area, in *2007 IEEE Particle Accelerator Conference (PAC): June 25-29, 2007* (IEEE, Albuquerque, NM, USA, 2007), pp. 2239–2241, https://ieeexplore.ieee.org/document/4441209.

[13] C. T. Rogers, D. Stratakis, G. Prior, S. Gilardoni, D. Neuffer, P. Snopok, A. Alekou, and J. Pasternak, Muon

front end for the neutrino factory, Phys. Rev. Accel. Beams **16**, 040104 (2013).

[14] D. Stratakis, H. K. Sayed, C. T. Rogers, A. Alekou, and J. Pasternak, Conceptual design and modeling of particle-matter interaction cooling systems for muon based applications, Phys. Rev. Accel. Beams **17**, 071001 (2014).

[15] J. W. Wang and G. A. Loew, *Field Emission and rf Breakdown in High-Gradient Room-Temperature Linac Structures* (Stanford Univ., Stanford Linear Accelerator Center, Menlo Park, CA, 1997), pp. 768–794, https://www.slac.stanford.edu/cgi-bin/getdoc/slac-pub-7684.pdf.

[16] W. Wuensch, Advances in the understanding of the physical processes of vacuum breakdown, in *High Gradient Accelerating Structure* (World Scientific, Singapore, 2014), pp. 31–50.

[17] Z. Insepov and J. Norem, Can surface cracks and unipolar arcs explain breakdown and gradient limits?, J. Vac. Sci. Technol. A **31**, 011302 (2013).

[18] A. Grudiev, S. Calatroni, and W. Wuensch, New local field quantity describing the high gradient limit of accelerating structures, Phys. Rev. Accel. Beams **12**, 102001 (2009).

[19] V. Dolgashev, S. Tantawi, Y. Higashi, and B. Spataro, Geometric dependence of radio-frequency breakdown in normal conducting accelerating structures, Appl. Phys. Lett. **97**, 171501 (2010).

[20] L. Laurent, S. Tantawi, V. Dolgashev, C. Nantista, Y. Higashi, M. Aicheler, S. Heikkinen, and W. Wuensch, Experimental study of rf pulsed heating, Phys. Rev. Accel. Beams **14**, 041001 (2011).

[21] K. Nordlund and F. Djurabekova, Defect model for the dependence of breakdown rate on external electric fields, Phys. Rev. Accel. Beams **15**, 071002 (2012).

[22] T. Luo, A. DeMello, A. Lambert, D. Li, S. Prestemon, and S. Virostek, Progress on the MICE 201 MHz cavities at LBNL, in *Proceedings, 6th International Particle Accelerator Conference (IPAC 2015): May 3-8, 2015* (JACoW Publishing, Richmond, Virginia, USA, 2015), p. WEPTY046.

[23] K. Yonehara, Recent progress of RF cavity study at Mucool Test Area, J. Phys. Conf. Ser. **408**, 012062 (2013).

[24] Y. Torun and A. Moretti, Grid window tests on an 805-MHz pillbox cavity, in *Proceedings, 6th International Particle Accelerator Conference (IPAC 2015): May 3-8, 2015* (JACoW Publishing, Richmond, VA, USA, 2015), p. WEPTY054.

[25] A. Kochemirovskiy, D. Bowring, Y. Torun, M. Chung, A. Moretti, P. Hanlet, G. Kazakevich, K. Yonehara, D. Peterson, G. Flanagan *et al.*, Breakdown characterization in 805 MHz pillbox-like cavity in strong magnetic fields, in *Proceedings, 6th International Particle Accelerator Conference (IPAC 2015): May 3-8, 2015*, WEPTY030 (JACoW Publishing, Richmond, VA, USA, 2015).

[26] M. Chung, M. G. Collura, G. Flanagan, B. Freemire, P. M. Hanlet, M. R. Jana, R. P. Johnson, D. M. Kaplan, M. Leonova, A. Moretti, M. Popovic, T. Schwarz, A. Tollestrup, Y. Torun, and K. Yonehara, Pressurized H_2 rf cavities in ionizing beams and magnetic fields, Phys. Rev. Lett. **111**, 184802 (2013).

[27] B. Freemire, M. Chung, P. Hanlet, R. Johnson, A. Moretti, Y. Torun, and K. Yonehara, The experimental program for high pressure gas filled radio frequency cavities for muon cooling channels, J. Inst. **13**, P01029 (2018).

[28] D. Stratakis, J. C. Gallardo, and R. B. Palmer, Effects of external magnetic fields on the operation of high-gradient accelerating structures, Nucl. Instrum. Methods Phys. Res., Sect. A **620**, 147 (2010).

[29] R. H. Fowler and L. Nordheim, Electron emission in intense electric fields, Proc. R. Soc. A **119**, 173 (1928).

[30] R. B. Palmer, R. C. Fernow, J. C. Gallardo, D. Stratakis, and D. Li, rf breakdown with external magnetic fields in 201 and 805 MHz cavities, Phys. Rev. Accel. Beams **12**, 031002 (2009).

[31] J. V. Beck, K. D. Cole, A. Haji-Sheikh, and B. Litkouhi, *Heat Conduction Using Green's Functions* (Hemisphere Publishing Corporation, London, 1992).

[32] D. P. Pritzkau and R. H. Siemann, Experimental study of rf pulsed heating on oxygen free electronic copper, Phys. Rev. Accel. Beams **5**, 112002 (2002).

[33] M. Bogomilov *et al.* (The MICE Collaboration), Lattice design and expected performance of the Muon Ionization Cooling Experiment demonstration of ionization cooling, Phys. Rev. Accel. Beams **20**, 063501 (2017).

[34] Z. Li, L. Ge, C. Adolphsen, D. Li, and D. Bowring, Improved rf design for an 805 MHz pillbox cavity for the U.S. MuCool program, in *Proceedings, 15th Advanced Accelerator Concepts Workshop (AAC 2012): June 10-15, 2012*, Vol. 1507 (AIP, New York, 2012), pp. 837–842.

[35] K. Ko, A. Candel, L. Ge, A. Kabel, R. Lee, Z. Li, C. Ng, V. Rawat, G. Schussman, and L. Xiao, Advances in parallel electromagnetic codes for accelerator science and development, in *Proc. Linear Accelerator Conference (LINAC2010)*, FR101 (JACoW Publishing, Tsukuba, Japan, 2010), https://accelconf.web.cern.ch/LINAC2010/papers/fr101.pdf; L. Ge, K. Ko, O. Kononenko, Z. Li, C.-K. Ng, and L. Xiao, Advances in parallel finite element code suite ACE3P, in *Proc. of 6th International Particle Accelerator Conference (IPAC2015)* (JACoW Publishing, Richmond, VA, USA, 2015), http://accelconf.web.cern.ch/IPAC2015/papers/mopmn002.pdf.

[36] M. Kuchnir and E. Hahn, Coating power RF components with TiN, Fermi National Accelerator Lab. Technical Report No. FERMILAB-TM-1928, 1995.

[37] K. Leung, Y. Lee, A. Mashaw, D. Wutte, and R. Gough, TiN coating of accelerator beamline chambers, in *Particle Accelerator Conference, 1997. Proceedings of the 1997*, FERMILAB-CONF-13-167-AD (IEEE, New York, 1997), pp. 3737–3739.

[38] D. W. Peterson and Y. Torun, Fermilab MuCool test area cavity conditioning control using LabVIEW, in *1st North American Particle Accelerator Conference (NAPAC2013)* (JACoW Publishing, Pasadena, CA, USA, 2013), https://lss.fnal.gov/archive/2013/conf/fermilab-conf-13-167-ad.pdf.